Lyapunov instabilities of Lennard-Jones fluids

Hong-liu Yang* and Günter Radons†
Institute of Physics, Chemnitz University of Technology, D-09107 Chemnitz, Germany
(Received 19 March 2004; revised manuscript received 16 November 2004; published 17 March 2005)

Recent work on many-particle systems reveals the existence of regular collective perturbations corresponding to the smallest positive Lyapunov exponents (LEs), called hydrodynamic Lyapunov modes. Until now, however, these modes have been found only for hard-core systems. Here we report results on Lyapunov spectra and Lyapunov vectors (LVs) for Lennard-Jones fluids. By considering the Fourier transform of the coordinate fluctuation density $u^{(\alpha)}(x,t)$, it is found that the LVs with $\lambda \approx 0$ are highly dominated by a few components with low wave numbers. These numerical results provide strong evidence that hydrodynamic Lyapunov modes do exist in soft-potential systems, although the collective Lyapunov modes are more vague than in hard-core systems. In studying the density and temperature dependence of these modes, it is found that, when the value of the Lyapunov exponent $\lambda^{(\alpha)}$ is plotted as function of the dominant wave number k_{max} of the corresponding LV, all data from simulations with different densities and temperatures collapse onto a single curve. This shows that the dispersion relation $\lambda^{(\alpha)}$ vs k_{max} for hydrodynamical Lyapunov modes appears to be universal for the low-density cases studied here. Despite the wavelike character of the LVs, no steplike structure exists in the Lyapunov spectrum of the systems studied here, in contrast to the hard-core case. Further numerical simulations show that the finite-time LEs fluctuate strongly. We have also investigated localization features of LVs and propose a length scale to characterize the Hamiltonian spatiotemporal chaotic states.

DOI: 10.1103/PhysRevE.71.036211 PACS number(s): 05.45.−a, 05.20.−y, 02.70.Ns, 05.45.Jn

I. INTRODUCTION

One of the most successful theories in modern science is statistical mechanics, which allows one to understand the macroscopic (thermodynamic) properties of matter from a statistical analysis of the microscopic (mechanical) behavior of the constituent particles. In spite of this, using certain probabilistic assumptions such as Boltzmann's *Stosszahlansatz* renders the lack of a firm foundation of this theory, especially for nonequilibrium statistical mechanics. Fortunately, the concept of chaotic dynamics developed in the 20th century [1] is a good candidate for coping with these difficulties. Instead of the probabilistic assumptions, the dynamical instability of trajectories can provide the necessary fast loss of time correlations, ergodicity, mixing, and other dynamical randomness [2]. It is generally expected that dynamical instability is at the origin of macroscopic transport phenomena and that one can find certain connections between them. In the past decade, some beautiful theories in this direction have already been developed. Examples are the escape-rate formalism by Gaspard and Nicolis [3,4] and the Gaussian thermostat method due to Nosé, Hoover, Evans, Morriss, and others [5–7], where the Lyapunov exponents were related to certain transport coefficients.

Very recently, molecular dynamics simulations on hard-core systems revealed the existence of regular collective perturbations corresponding to the smallest positive Lyapunov exponents (LEs), named hydrodynamic Lyapunov modes [8]. This opens a possible way for a connection between Lyapunov vectors, quantities characterizing the dynamical instability of trajectories, and macroscopic transport properties. A lot of work [9–16] has been done to identify this phenomenon and to find its origin. It is commonly thought that the appearance of these modes is due to the conservation of certain quantities in the systems studied [10–14]. A natural consequence of this expectation is that the appearance of such modes would not be an exclusive feature of hard-core systems and should be generic to a large class of Hamiltonian systems. However, until now, these modes have been identified only in computer simulations of hard-core systems [9,10,16].

In this work, we report results about a one-dimensional (1D) system with Lennard-Jones interaction. Although the identification of regular hydrodynamic Lyapunov modes by the naked eye is difficult for soft-potential systems [16], our technique based on a spectral analysis of Lyapunov vectors (LVs) shows strong evidence that hydrodynamic Lyapunov modes do exist in this case. The influence of density and temperature changes is studied in detail. The dispersion relation for hydrodynamic Lyapunov modes, the dominant wave number as a function of the corresponding LEs, is found to have a quite weak dependence on the densities and temperatures used.

Furthermore we study the localization properties of LVs. Based on the extensive nature of LVs with $\lambda \approx 0$, we propose a length scale to characterize a spatiotemporal chaotic Hamiltonian system. It is expected that this quantity will be useful for the task of distinguishing different spatiotemporal chaotic states and characterizing transitions among them. This is an important open question in the study of spatiotemporal chaos [17].

II. MODEL

In this study we use a 1D Lennard-Jones system with Hamiltonian

*Electronic address: hongliu.yang@physik.tu-chemnitz.de
†Electronic address: radons@physik.tu-chemnitz.de

$$H = \sum_{i=1}^{N} mv_i^2/2 + \sum_{i<j} V(x_j - x_i). \quad (1)$$

The interaction potential among particles is of the form

$$V(r) = \begin{cases} 4\epsilon\left[\left(\frac{\sigma}{r}\right)^{12} - \left(\frac{\sigma}{r}\right)^{6}\right] - V_c & \text{if } r \leqslant r_c, \\ 0 & \text{otherwise}, \end{cases} \quad (2)$$

with $V_c = 4\epsilon[(\sigma/r_c)^{12} - (\sigma/r_c)^6]$. The potential is truncated in order to lower the computational burden. Note, however, that due to the truncation the force $f(r) \equiv -V'(r)$ and its derivative $f'(r)$ are not continuous at the truncation point r_c. This will introduce additional noise in the numerical integration of the equation of motion and the corresponding tangent dynamics. For this reason, two other potentials with continuous derivatives at the truncation point were also simulated to check the influence on the results given below. The first one was proposed by Stoddard and Ford [18]. It is continuous in the force at the truncation point,

$$V(r) = \begin{cases} 4\epsilon\left[\left(\frac{\sigma}{r}\right)^{12} - \left(\frac{\sigma}{r}\right)^{6}\right] + c_2\left(\frac{r}{r_c}\right)^2 + V_c & \text{if } r \leqslant r_c, \\ 0 & \text{otherwise}, \end{cases} \quad (3)$$

with $c_2 = 4\epsilon[6(\sigma/r_c)^{12} - 3(\sigma/r_c)^6]$ and $V_c = 4\epsilon[-7(\sigma/r_c)^{12} + 4(\sigma/r_c)^6]$. The second potential used is continuous in addition in the first derivative of the force and it is of the form

$$V(r) = 4\epsilon\left[\left(\frac{\sigma}{r}\right)^{12} - \left(\frac{\sigma}{r}\right)^{6}\right] + c_4\left(\frac{r}{r_c}\right)^4 + c_2\left(\frac{r}{r_c}\right)^2 + V_c \quad (4)$$

for $r \leqslant r_c$, and $V(r) = 0$ otherwise. The constants are given by $c_4 = 4\epsilon[-21(\sigma/r_c)^{12} + 6(\sigma/r_c)^6]$, $c_2 = 4\epsilon[48(\sigma/r_c)^{12} - 15(\sigma/r_c)^6]$, and $V_c = 4\epsilon[-28(\sigma/r_c)^{12} + 10(\sigma/r_c)^6]$. Using the same integration step size, the latter two potentials [Eqs. (3) and (4)] typically yield better numerical accuracy than the first one [Eq. (2)]. This will somewhat influence the quality of the zero-value Lyapunov exponents. The qualitative behaviors of the Lyapunov modes, however, turn out to be not affected by the above modifications of the potential (see the Appendix).

The system is integrated using the velocity form of the Verlet algorithm with periodic boundary conditions [19]. In our simulations, we set $m = 1$, $\sigma = 1$, $\epsilon = 1$, and $r_c = 2.5$. All results are given in reduced units, i.e., length in units of σ, energy in units of ϵ, and time in units of $(m\sigma^2/48\epsilon)^{1/2}$. The time step used in the molecular dynamics simulation is $h = 0.008$. The standard Gram-Schmidt reorthonormalization algorithm [20,21] is used to calculate the local dynamical instability of the systems studied. The time interval for periodic reorthonormalization is $30h$ to $100h$. Throughout this paper, the particle number typically is denoted by N, the length of the system by L, and the temperature by T.

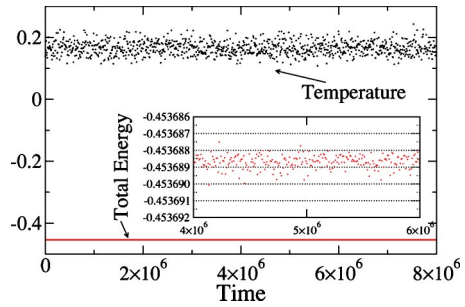

FIG. 1. Time evolution of temperature $T \equiv \langle mv^2 \rangle$ and total energy. The inset shows that the total energy E has small short-term fluctuations but no long-term drift. Detailed calculation shows that the standard deviation of the total energy $\sigma(E) = 4 \times 10^{-7}$. The nearly constant state variables show that the system has already reached a stationary state. The parameter settings used here are $N = 100$, $L = 1000$, and $T = 0.2$.

III. NUMERICAL RESULTS

A. The stationary state

In the numerical calculation of the Lyapunov instability of a many-body system [22], there are some important time scales to be kept in mind: the first one is the time for a many-body system to relax to a stationary state, which guarantees that quantities measured afterward are not for a transient state; the second is the time for the set of Lyapunov vectors to relax to their correct orientations since offset vectors are usually selected randomly at the beginning; the third is the time used to count LEs and LVs, which should be long enough to ensure that the trajectory wanders all over the attractor. For a many-body system like the one studied here, these time scales can be extremely long due to the large number of degrees of freedom involved [23,24].

The time evolution of state variables like temperature T and total energy for a case with parameter settings $N = 100$, $L = 1000$, and $T = 0.2$ is shown in Fig. 1. In the beginning of our molecular dynamics simulation, particles are placed randomly in the interval $[0, L]$. Their velocities are chosen randomly from a Boltzmann distribution. In order to equilibrate the system, it is coupled to a stochastic heat bath with given temperature T, i.e., every 500 steps the velocities of the particles are replaced with velocities that were drawn from a Boltzmann distribution corresponding to that temperature. This was done for a time period of length t_{eq}, which is longer than the relaxation time of the system at this temperature. After the equilibration procedure, the system is allowed to evolve with constant total energy, i.e., without the heat bath, for a time period of the same length as t_{eq}, in order to be sure that the system is already in a stationary state at given temperature T. In Fig. 1, the period with the thermal bath is omitted and only the part of the evolution with constant total energy is shown. The nearly constant value of temperature means that the system has already reached a stationary state and one can start the calculation of the Lyapunov instability of the system. In the inset of Fig. 1, one can see that there exist short-term fluctuations in the total energy. The energy fluctuations are mainly due to the discretization of the evolution equations for the numerical integration. In general, the

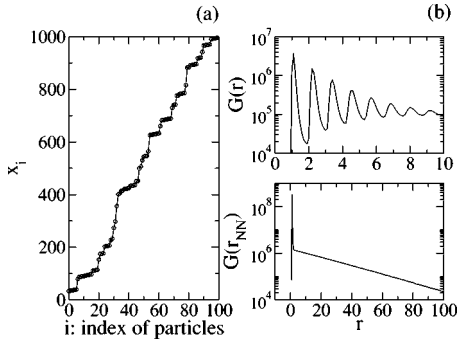

FIG. 2. (a) Snapshot of the particle positions x_i vs index of particles i and (b) pair distribution function $G(r)$ obtained from the distances between all particles (upper panel) and from nearest neighbors only (lower panel) for the stationary state shown in Fig. 1 [see [25] for the definition of $G(r)$]. The sharp peaks in $G(r)$ imply that the state is a broken-chain state.

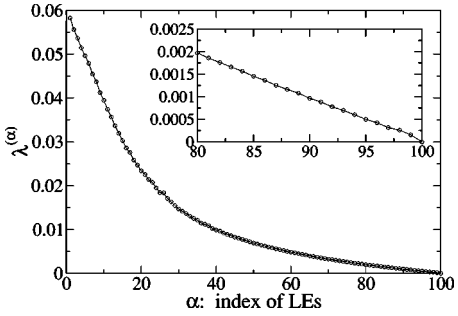

FIG. 3. Lyapunov spectrum for the state shown in Fig. 2. Enlargement of the part in the regime $\lambda^{(\alpha)} \approx 0$ is shown in the inset. It is the result of an average over 58 samples with different initial conditions and for each sample the averaging period is $4 \times 10^6 h$. Here no stepwise structure exists, in contrast to the case of hard-core systems. This is a typical result for our soft-potential system.

discretized equations can be regarded as resulting from a periodically kicked system, implying that the evolution is no longer autonomous. The amplitude of the numerical error caused by this effect in general depends on the integration algorithm used. Our preference for the standard velocity Verlet algorithm, although it is of lower order than the typical fourth-order Runge-Kutta algorithm, is due to its property of preserving time reversibility and phase space volumes. These properties ensure that the Verlet algorithm shows little long-term drift in the total energy although its short-time fluctuations may be larger than for Runge-Kutta integrators [26]. An additional difficulty faced in the numerical integration is the discontinuity in the derivatives of the potential caused by its truncation. Here the flowing in and out of the interaction range of particles leads to additional numerical noise. In general, decreasing the integration step size can reduce the effect of numerical errors and improve the accuracy of the energy conservation. This is also confirmed by our numerical simulations (see the Appendix). A smaller step size, however, means that more integration steps are needed to simulate a fixed length trajectory. Limited by the capacity of our computers, we are forced to select an integration step size that minimizes the total error resulting on one hand from too short trajectories and on the other hand from the finite step size.

The pair distribution function $G(r)$ shown in Fig. 2 tells us that the stationary state for $T=0.2$ is a broken-chain state with short-range order. This is generic for a 1D Lennard-Jones system with not too high density [27].

B. Benettin method using Gram-Schmidt orthogonalization

The standard method invented by Benettin *et al.* [20] and Shimada and Nagashima [21] is the most efficient one to calculate the Lyapunov exponents and Lyapunov vectors of large systems. Here $N \times N$ linearized equations for N offset vectors in tangent space were integrated simultaneously with the set of N nonlinear equations for the reference trajectory. Offset vectors were periodically reorthonormalized using the Gram-Schmidt algorithm. The resulting rescaling factors measure the expansion or contraction rate of offset vectors in certain directions. Averaging their logarithms for a period τ gives what are called *finite-time Lyapunov exponents* λ_τ. The limit $\lambda \equiv \lambda_{\tau \to +\infty}$ is what is usually called the *Lyapunov exponent*. The value of a finite-time LE λ_τ depends on the trajectory segment where it is calculated and usually it fluctuates as the segment moves along the trajectory. However $\lambda_{+\infty}$ is time independent and unique for an ergodic system. In this sense, $\lambda_{+\infty}$ is a global quantity characterizing the system attractor, while the finite-time LEs are local quantities which contain more detailed information about the dynamics. The offset vectors just after reorthonormalization are called *Lyapunov vectors*. These are local quantities characterizing the system attractor similar to the finite-time LEs.

Another point to be noted is that Lyapunov vectors obtained using Benettin *et al.*'s method are always mutually orthogonal while the local unstable and stable directions are not orthogonal in general. In this sense, these are two different sets of vectors. They are also different from the ones in the multiplicative ergodic theorem [28]. However, recent study shows that they are indirectly related to the set of Oseledec vectors [29]. Lyapunov vectors obtained in the standard way can at least represent the most unstable direction in a certain subspace and they already contain a lot of important information about the dynamical instability in tangent space. We will rely on them to continue our study in this paper.

C. Finite-time Lyapunov exponents with wild fluctuations

The Lyapunov spectrum for the case with $N=100$, $L=1000$, and $T=0.2$ is shown in Fig. 3. Here only half of the spectrum is shown since all LEs of Hamiltonian systems come in pairs according to the conjugate-pairing rule [30,31]. From the enlargement shown in the inset of Fig. 3 for the part near $\lambda^{(\alpha)} \approx 0$, one cannot see any stepwise structure in the Lyapunov spectrum in contrast to the case of hard-core systems [10]. This is the typical result obtained for our soft-potential system.

From Fig. 3 it is tempting to conclude that there is only one zero-value Lyapunov exponent in the part of the spec-

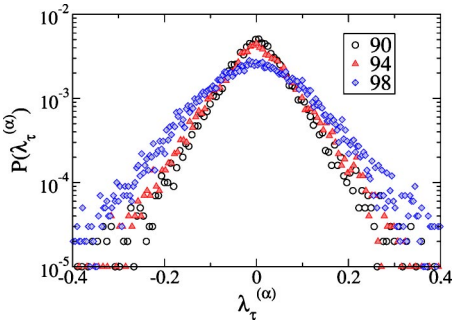

FIG. 4. Distribution of the finite-time Lyapunov exponent $\lambda_\tau^{(\alpha)}$ where τ is equal to the period of reorthonormalization and the index of LEs α is equal to 90, 94, and 98, respectively. The strong fluctuations of $\lambda_\tau^{(\alpha)}$ are one of the possible reasons for the disappearance of the stepwise structures in the Lyapunov spectrum. The parameter settings used here are $N=100$, $L=1000$, and $T=0.2$.

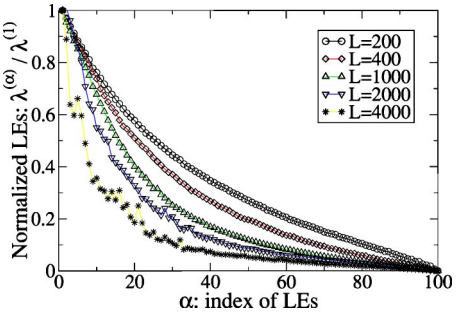

FIG. 5. Normalized Lyapunov exponents $\lambda^{(\alpha)}/\lambda^{(1)}$ with $L=200$, 400, 1000, 2000, and 4000, respectively. The Lyapunov spectrum becomes more and more bent as the particle density $\rho=N/L$ is decreased. This implies the separation of two time scales. Here $N=100$ and $T=0.2$.

trum shown. This seems to contradict the expectation that there should be two due to the conservation laws [10,12,14]. Our detailed studies of these Lyapunov exponents and the corresponding Lyapunov vectors show that there are indeed four zero-value Lyapunov exponents (two in the part shown). The point is that two of them ($\lambda^{(99)}$ and $\lambda^{(102)}$) are more sensitive to numerical errors than the other two ($\lambda^{(100)}$ and $\lambda^{(101)}$). The two exponents corresponding to translational invariance in space and momentum conservation are closer to zero since these properties are preserved exactly in the numerical integration routine. The other pair of Lyapunov exponents, which show relatively large deviations from zero, correspond to energy conservation and translational invariance in time. These properties are not preserved exactly by the numerical discretization of the governing equations of motion. Correspondingly, fluctuations in the total energy are introduced by the numerical integration (see Fig. 1) and in consequence lead to the observed deviation from zero of this pair of Lyapunov exponents. In principle, one can improve the results for this pair of Lyapunov exponents (i.e., bring them closer to zero) by reducing the integration step size. The main limitation comes from the capacity of the computational resource because one needs to integrate over very long time periods. In order to support this point of view we performed extensive numerical simulations for small systems with few particles. The details of this analysis are provided in the Appendix. Our numerical results show also that the quality of this pair of LEs is sensitive to the details of the integration scheme, while the behavior of the Lyapunov modes is quite robust.

The fluctuations in local instabilities of trajectories are demonstrated by the distribution of finite-time LEs. In Fig. 4 such distributions for some LEs in the regime $\lambda \approx 0$ are presented. Fluctuations of the finite-time Lyapunov exponents are quite large compared with the difference between their mean values, i.e., $\sigma(\lambda_\tau^{(\alpha)}) \equiv \sqrt{\langle \lambda_\tau^{(\alpha)2} \rangle - \langle \lambda_\tau^{(\alpha)} \rangle^2} \gg |\lambda^{(\alpha)} - \lambda^{(\alpha+1)}|$. Here $\langle \cdots \rangle$ means the time average. The strong fluctuation in local instabilities is one of the possible reasons for the disappearance of the stepwise structures in the Lyapunov spectra. It could also cause the mixing of nearby Lyapunov vectors. The mixing may be at the origin of the intermittency observed in the time evolution of the spatial Fourier transform of LVs (see Sec. III E).

D. Bending of Lyapunov spectrum with decreasing particle density

We studied also the influence of the particle density on the Lyapunov spectrum by increasing the length of the system with the particle number N kept fixed. As can be seen in Fig. 5, the Lyapunov spectrum becomes more and more bent with increasing L. For the case of $L=4000$, the spectrum can already be unambiguously divided into two regimes: In the upper regime, Lyapunov exponents decrease more quickly with increasing index than in the lower regime. Such a bending of the Lyapunov spectrum was related to the separation of two time scales in dilute particle systems [32]. Our conjecture is that one is the time of local collision events, and the other is due to the collective motion of the particles. Support for this conjecture comes from our results presented in Sec. III E 4. For a system with high density, the collisions are so frequent that there are strong correlations between consecutive collisions and one can no longer separate them from each other. The collisions themselves contribute to the collective motion of the system. Therefore no time scale separation happens here and the LEs decrease gradually.

E. Spatial structure of LVs with $\lambda^{(\alpha)} \approx 0$

1. Coordinate fluctuation density

Another quantity used to characterize the local instability of trajectories is the Lyapunov vector $\delta\Gamma^{(\alpha)}$, which represents expanding or contracting directions in tangent space. In the study of hard-core systems, Posch and co-workers found that the coordinate parts of the Lyapunov vectors corresponding to $\lambda \approx 0$ are of regular wavelike character [8–10]. They are referred to as *hydrodynamic Lyapunov modes*. We are searching here for the counterpart of these modes in our soft-potential system.

Remember that each of the LVs consists of two parts: the displacements δx_i in coordinate space and δv_i in momentum space. In past studies of hydrodynamic Lyapunov modes in hard-core systems, only the coordinate part δx_i was consid-

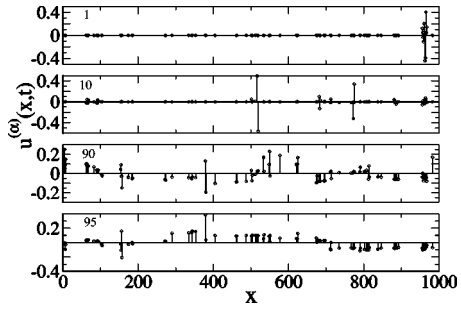

FIG. 6. $u^{(\alpha)}(x,t)$ for LVs with index $\alpha=1$, 10, 90, and 95, respectively. $u^{(\alpha)}(x,t)$ is visualized by plotting vertically the fluctuations $\delta x_i^{(\alpha)}$ at the corresponding positions x_i along the x axis. Notice that the LVs with $\alpha=1$ and 10 are more localized while those with $\alpha=90$ and 95 are more distributed. The parameter settings used here are $N=100$, $L=1000$, and $T=0.2$.

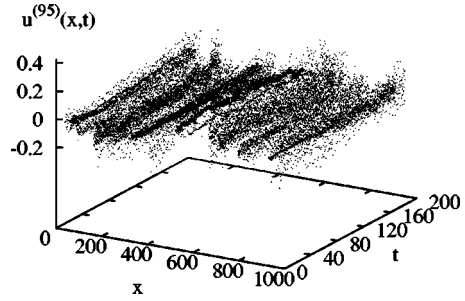

FIG. 7. Time evolution of $u^{(95)}(x,t)$ for parameters as in Fig. 6. No clear wave structure can be detected.

ered. This is due to an interesting feature of hydrodynamic Lyapunov modes found in Ref. [12] which says that the angles between the coordinate part and the momentum part are always small, i.e., the two vectors are nearly parallel. Therefore, it is already sufficient to use only δx_i for studying $\delta\Gamma$. For our soft-potential system, we find that the angles between the coordinate part and the momentum part are no longer as small as in the hard-core systems. However, we will still follow the tradition of studying the coordinate part of the LV first and come to the momentum part afterward.

Analogous to the definition of microscopic densities in hydrodynamics [25], we define a quantity called the *coordinate fluctuation density* (CFD)

$$u^{(\alpha)}(x,t)=\sum_{i=1}^{N}\delta x_i^{(\alpha)}\delta(x-x_i). \tag{5}$$

Profiles of $u^{(\alpha)}(x,t)$ for some typical LVs of the Lennard-Jones system are presented in Fig. 6. It can be seen that $u^{(\alpha)}(x,t)$'s for LVs corresponding to the largest Lyapunov exponents are highly localized, for example $u^{(1)}(x,t)$ and $u^{(10)}(x,t)$, while those for LV_{90} and LV_{95} are more distributed. The study of the localization of LV_1, the LV corresponding to the largest Lyapunov exponent, is of long history [9,10,32–37] and it was related, e.g., to defect events in simulations of Benard convection [36]. We leave the discussion on this point to Sec. III F. The temporal evolution of $u^{(95)}(x,t)$ is shown in Fig. 7 in order to make the possibly existing wavelike structure more evident. A wave structure, however, cannot unambiguously be detected here with the naked eye.

2. Spatial power spectrum of CFD and intermittency in its time evolution

Now we turn to the spatial Fourier transform of $u^{(\alpha)}(x,t)$, which reads

$$\tilde{u}_k^{(\alpha)}(t)=\int u^{(\alpha)}(x,t)\exp(-ik\cdot x)dx=\sum_{j=1}^{N}\delta x_j^{(\alpha)}\exp[-ik\cdot x_j(t)]. \tag{6}$$

In previous studies, in order to make the wave structure more obvious, certain smoothing procedures in time or space were applied to the Lyapunov vectors. For a $1d$ hard-core system with only a few particles, this procedure has been shown to be quite useful in identifying the existence of hydrodynamic Lyapunov modes [15]. The success of this strategy relies on the fact that some of the hydrodynamic Lyapunov modes (transverse modes) of hard-core systems are stationary [8]. Therefore, time averaging can indeed suppress the noise component and make the long-wavelength modes more significant. For a soft-potential system, all the Lyapunov vectors are not stationary due to the random mixing among them. In particular, for our one-dimensional system studied here, no transverse modes but only longitudinal Lyapunov modes exist. In consequence of this, the smoothing procedure is no longer helpful for detecting the hidden regular modes and can even damage them [16]. Here we apply the spatial Fourier transformation to the instantaneous quantity $u^{(\alpha)}(x,t)$ instead. The algorithm offered especially for unevenly distributed data is very suitable for our case [38]. Furthermore, we take the long-time average (and ensemble average) of the instantaneous spatial Fourier spectrum

$$s_{uu}^{(\alpha)}(k,t)\equiv|\tilde{u}_k^{(\alpha)}(t)|^2 \tag{7}$$

since it is expected that in $S_{uu}^{(\alpha)}(k)\equiv\langle s_{uu}^{(\alpha)}(k,t)\rangle$ the contribution of stochastic fluctuations will be averaged out while the information about the collective modes will be left and accumulated. The following results show that this technique is quite successful in detecting the hidden collective modes.

The time evolution of the instantaneous spatial Fourier spectrum $s_{uu}^{(95)}(k,t)$ for Lyapunov vector no. 95 is shown in Fig. 8 as an example. Two quantities are recorded with increasing time. One is the peak wave number k_*, which marks the position of the highest peak in the spectrum $s_{uu}^{(\alpha)}(k,t)$ (see Fig. 9). The other is the spectral entropy $H_s(t)$ [39], which measures the distribution property of the spectrum $s_{uu}^{(\alpha)}(k,t)$. It is defined as

$$H_s(t)=-\sum_{k_i}s_{uu}^{(\alpha)}(k_i,t)\ln s_{uu}^{(\alpha)}(k_i,t). \tag{8}$$

A smaller value of $H_s(t)$ means that the spectrum $s_{uu}^{(\alpha)}(k,t)$ is highly concentrated on a few values of k, i.e., these components dominate the behavior of the LV. Both of these quan-

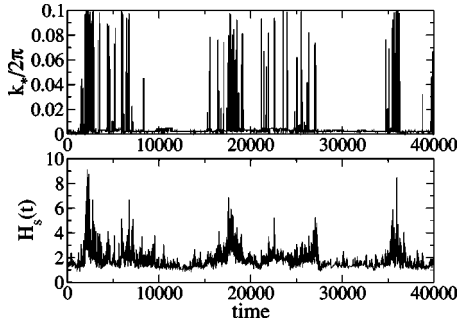

FIG. 8. Intermittent behavior of the peak wave number k_* and spectral entropy $H_s(t)$ for the spatial Fourier spectrum of $u^{(95)}(x,t)$. The parameter settings used here are $N=100$, $L=1000$, and $T=0.2$.

tities behave intermittently as shown in Fig. 8. Large intervals of nearly constant low values (off state) are interrupted by short period of bursts (on state) where they experience large values. Details of typical on and off states are shown in Fig. 9. It can be seen that the off state is dominated by the low-wave-number components (see the sharp peak at low wave number k_*) while the on state is more noisy and there are no significant dominant components. This intermittency in the time evolution of the spatial Fourier spectrum of LVs is a typical feature of soft-potential systems. It is conjectured that this is a consequence of the mixing of nearby LVs caused by the wild fluctuations of local instabilities. Due to the mutual interaction among modes, the hydrodynamic Lyapunov modes in soft-potential systems are only of finite lifetime. In the dynamic Lyapunov structure function estimated, the peak representing the propagating (or oscillating) Lyapunov modes is of finite width. This is a support of our conjecture that the hydrodynamic Lyapunov modes are of finite lifetime. Details of this study will be presented elsewhere [40].

Recently Eckmann *et al.* conjectured that the longitudinal Lyapunov modes came in pairs with the so-called P modes [41]. The dynamics of the Lyapunov modes were explained as a rotation with constant angular velocity in the subspace spanned by a certain LP pair. Numerical results for hard-core

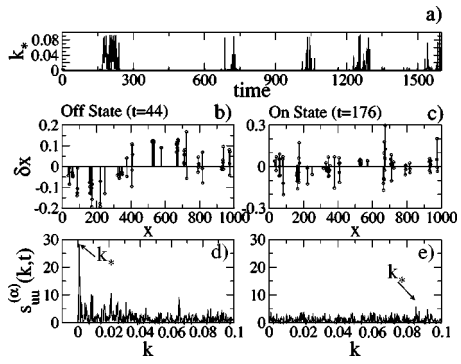

FIG. 9. (a) Variation of the peak wave number k_* with time. (b), (c) Two typical snapshots of LV_{95}, off and on states at $t=44$ and 176, respectively. (d),(e) Their spatial Fourier transforms. The spectrum for the off state has a sharp peak at small k_* while that for the on state has no dominant peak. The parameter settings used here are $N=100$, $L=1000$, and $T=0.2$.

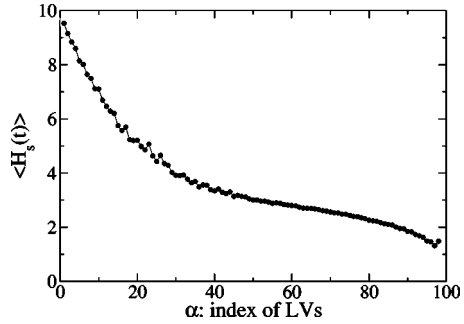

FIG. 10. Time-averaged spectral entropy $\langle H_s(t)\rangle$ vs index of LVs. The gradual decrease of $\langle H_s(t)\rangle$ from $\alpha\approx 0$ means that LVs corresponding to smaller positive LEs are more localized in Fourier space, i.e., they have more wavelike character, than those corresponding to larger LEs. The parameter settings used here are $N=100$, $L=1000$, and $T=0.2$.

systems were provided to support their conjecture. We expect that the proposed mechanism, possibly in a modified form, also works for the soft-potential system studied here. The strong mixing among Lyapunov modes in our system, however, makes the dynamics of the modes more complex than in the hard-core systems. If only mixing between the modes in the same LP pair were possible as in hard-core systems, a regular periodic oscillation instead of the irregular intermittency behavior in k_* would be expected. Therefore we think that the observed intermittency in the dynamics of the Lyapunov modes is the combined effect of the rotation and the finite lifetime of the modes.

In Fig. 10, the time-averaged spectral entropy $\langle H_s(t)\rangle$ is plotted against the index of the LVs. It increases gradually as the index decreases from $N-2$. This means that LVs corresponding to smaller positive LEs are more localized in Fourier space, i.e., they have more wavelike character, than those corresponding to larger LEs.

3. Dispersion relation of hydrodynamic Lyapunov modes

Now we consider the time-averaged spatial Fourier spectrum $S_{uu}^{(\alpha)}(k)$ of LVs. Two cases with $L=1000$ and 2000 are shown in Fig. 11. It is not hard to recognize the sharp peak at $\lambda\approx 0$ in the contour plot of the spectrum. In increasing the Lyapunov exponents, the peak shifts to the larger-wave-number side. A dashed line is plotted to show how the wave number of the peak k_{max} changes with $\lambda^{(\alpha)}$. To further demonstrate this point, in Fig. 12, the value of the Lyapunov exponent $\lambda^{(\alpha)}$ is plotted versus k_{max} of the corresponding LVs. We call this the *dispersion relation* of the hydrodynamical Lyapunov modes. The numerical fitting of the data shows that for $\lambda\approx 0$, $\lambda^{(\alpha)}\sim k_{max}^{\gamma}$ with the exponent $\gamma\approx 1.2$. We conjecture that a linear dispersion relation $\lambda^{(\alpha)}\sim k_{max}$ may be obtained as the thermodynamic limit is approached and the deviation from the linear function of the data shown in Fig. 12 is due to finite-size effects.

In order to show that the peak in $S_{uu}^{(\alpha)}(k)$ is not a result of the highly regular packing of particles in the broken-chain state, the static structure function [25]

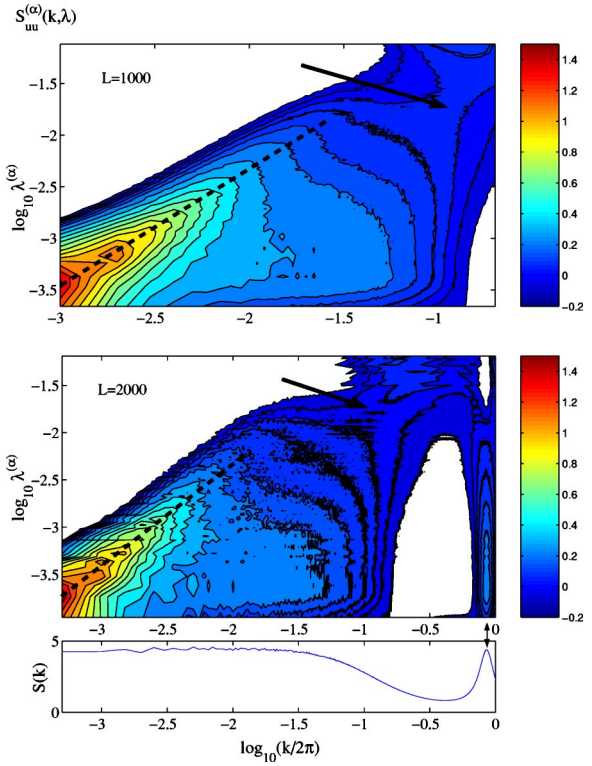

FIG. 11. (Color online) Contour plot of the spectrum $S^{(\alpha)}_{uu}(k)$ for $L=1000$ and 2000. There is a sharp peak at $k\approx 0$ and $\lambda\approx 0$. To guide eyes, a dashed line is plotted to show how the peak wave number k_{max} changes with the variation of λ. The sudden jump in k_{max} is marked with an arrow. In total 58 samples for the case of $L=1000$ (ten for $L=2000$) are used for averaging for each period of $4\times 10^6 h$. Here $T=0.2$ and $N=100$.

$$S(k) \equiv \int G(r)\exp(-ikr)dr \tag{9}$$

for the case $L=2000$ is plotted in the same figure as $S^{(\alpha)}_{uu}(k)$, where $G(r)$ is the pair correlation function shown in Fig. 2. It can be seen that $S(k)$ is nearly constant in the regime $k\approx 0$, the place where a sharp peak was observed in $S^{(\alpha)}_{uu}(k)$. The

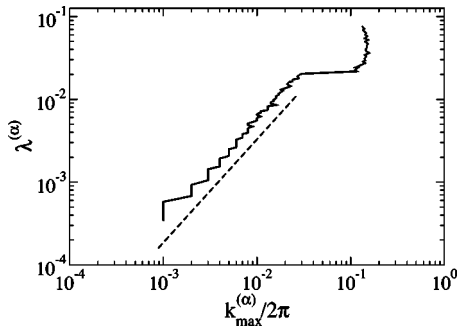

FIG. 12. The Lyapunov exponent $\lambda^{(\alpha)}$ is plotted as function of the wave number k_{max} of the highest peak in the time-averaged spatial Fourier spectrum of LVs. The dashed line is of the form $\lambda^{(\alpha)}\sim k^{1.2}_{max}$. The parameter settings used here are $N=100$, $L=1000$, and $T=0.2$.

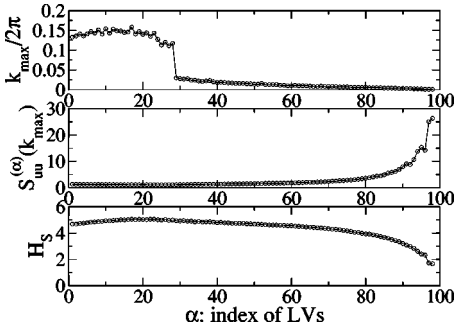

FIG. 13. (Top panel) The wave number k_{max} of the highest peak in the time-averaged spatial Fourier spectrum of LVs. (Middle panel) The height $S^{(\alpha)}_{uu}(k_{max})$ of the highest peak in the time-averaged spectrum. (Bottom panel) The spectral entropy H_S for the averaged spectrum $S^{(\alpha)}_{uu}(k)$. The sudden jump in k_{max} implies the separation of time scales. The parameter settings used here are $N=100$, $L=1000$, and $T=0.2$.

regular packing of particles causes the formation of a peak at $k/2\pi\approx 0.9$ in $S(k)$. This corresponds to a tiny peak at the same k value in $S^{(\alpha)}_{uu}(k)$ for those LVs with $\lambda\approx 0$. These facts show clearly that the collective modes observed in LVs are not due to the regular packing of particles.

To further demonstrate the properties of these modes, in Fig. 13, k_{max} is plotted versus the index of the LVs. As can be seen, for LVs with $\lambda\approx 0$, i.e., with $\alpha\approx N$, the value of k_{max} is quite small (see the enlargement in Fig. 14). For example, for $\alpha=96$, 97, and 98, $k_{max}=2\pi/L$, which is the smallest nonzero wave number allowed by the periodic boundary conditions used. Another point to be noticed is the step structure in plotting k_{max} as a function of α. This is similar to the degeneration of wave numbers found in the hard-core case, although the steps here are not so regular. In the middle panel of Fig. 13, the height $S^{(\alpha)}_{uu}(k_{max})$ of the highest peak in the time-averaged spatial spectrum is plotted as a function of the index of the LVs. Apart from LVs no. 99 and no. 100 (not shown) for the conserved quantities, $S^{(\alpha)}_{uu}(k_{max})$ decreases gradually in decreasing the index from $N-2$. Similarly to the definition of the spectral entropy for the instantaneous spectrum $s^{(\alpha)}_{uu}(k,t)$ in Eq. (8), one can also define a spectral entropy H_S for the averaged spectrum $S^{(\alpha)}_{uu}(k)$. The spectral entropy H_S for $S^{(\alpha)}_{uu}(k)$ is presented in the bottom panel of Fig. 13. It possesses a minimum at $\alpha=98$ where the Lyapunov

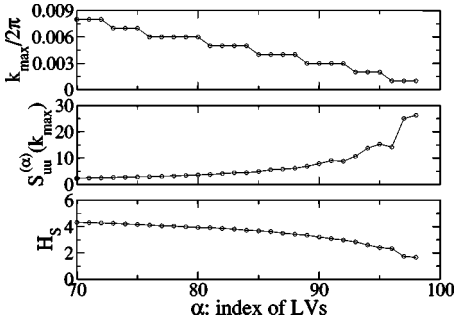

FIG. 14. Enlargement of Fig. 13 for the part in the regime $\alpha\simeq N$.

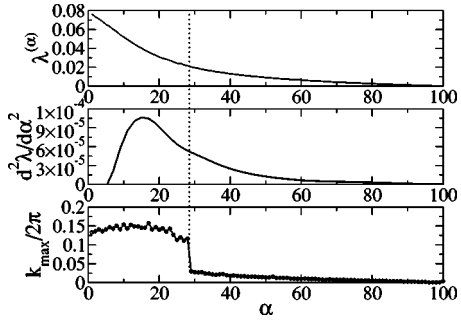

FIG. 15. The Lyapunov spectrum $\lambda^{(\alpha)}$ (top panel), $d^2\lambda/d\alpha^2$ (middle panel), and k_{max} (bottom panel) vs the index α. The parameter settings used here are $N=100$, $L=1000$, and $T=0.2$.

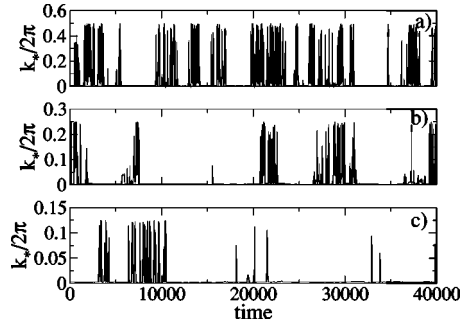

FIG. 16. Same as top panel of Fig. 8, but with different density $\rho=$(a) 1/2, (b) 1/4, and (c) 1/8, respectively. Here $T=0.2$ and the particle number $N=100$.

exponent is the smallest positive one. According to the definition of the spectral entropy, the minimum means that the spectrum of LV no. 98 is most significantly dominated by a few components.

All of our results shown above give strong evidence that the Lyapunov vectors corresponding to the smallest positive LEs in our 1D Lennard-Jones system are highly dominated by a few components with small wave numbers, i.e., they are similar to the hydrodynamic Lyapunov modes found in hard-core systems. The wavelike character becomes weaker and weaker as the value of the LE is increased gradually from zero.

4. Separation of time scales

Another interesting point in Fig. 13 is the sudden jump in k_{max} at $\alpha\approx 26$ which divides the whole set of LVs into two groups. It is believed that this sudden jump is related to the bending of the LE spectrum and the separation of time scales in a dilute system. As shown in Fig. 15, the sudden jump is in the regime where the LE spectrum is most strongly bent, although it is not at the exact place where $d^2\lambda^{(\alpha)}/d\alpha^2$ experiences the maximal value. Further work is needed to reveal the underlying connection between these phenomena.

5. Influence of density and temperature

To study how the change in density influences the behavior of LVs, we increase the length L of the system from 200 to 4000 with the particle number N kept fixed at 100. From the time evolution of k_* shown in Fig. 16, one sees that, in increasing the density $\rho=N/L$, the occurrence of the on state becomes more frequent, i.e., the domination of low-wave-number components is much weaker. The spatial Fourier spectra for LVs with LEs in the regime $\lambda^{(\alpha)}\simeq 0$, however, are always dominated by certain low-wave-number components irrespective of the density (see Fig. 17).

An important point is the collapse of data of dispersion relations from simulations with various densities and temperatures to a single curve (see bottom panel of Fig. 17). This means, for hydrodynamic Lyapunov modes in our system, that the dispersion function $\lambda_\alpha(k)$ is universal for the particle densities and the system temperatures studied. Fitting of the data to a power-law function $\lambda_\alpha\sim k_{max}^\gamma$ gives the value of the exponent γ as 1.2 ± 0.1 which is not far from a linear dispersion. Since our simulations here are limited to cases with relatively low density, the possibility of a density dependence of the dispersion relation cannot be excluded for high densities.

Another feature of Fig. 17 (bottom panel) is that the sudden jump in k_{max} disappears as the system density N/L is increased. This is consistent with our above discussion that the separation of time scales is significant only in dilute systems.

6. Dynamics of the momentum part

Now we turn to investigations of the spatial Fourier spectrum of the momentum part of LVs. Unfortunately, all the spectra are more or less homogeneously distributed on all

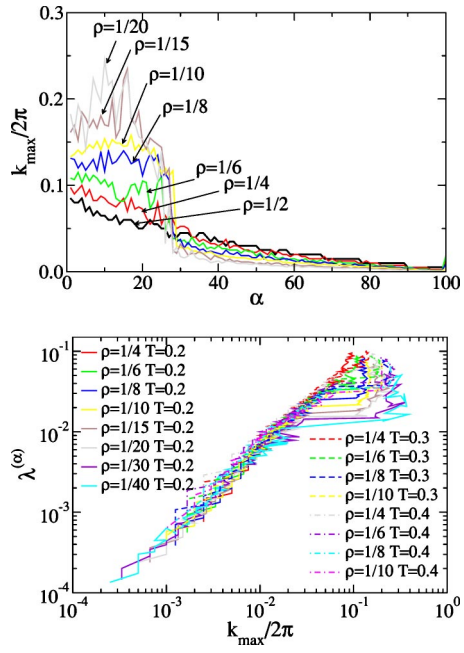

FIG. 17. (Color online) (Top panel) the wave number k_{max} of the highest peak in the time-averaged spatial Fourier spectrum of LVs as a function of LV index α. (Bottom Panel) the Lyapunov exponent $\lambda^{(\alpha)}$ as function of k_{max}. Note that in the bottom panel, all data from simulations with different densities and temperatures collapse to a single curve. Fitting of the low-wave-number part to a power-law function $\lambda^\alpha\sim k_{max}^\gamma$ gives $\gamma\approx 1.2\pm0.1$. Here $N=100$ and $T=0.2$.

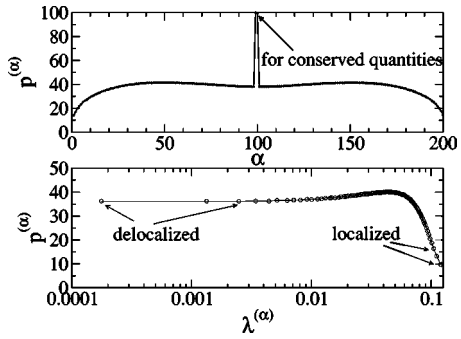

FIG. 18. Time-averaged participation number $p^{(\alpha)}$ vs index of LVs (upper panel) and $\lambda^{(\alpha)}$ (lower panel). The parameter settings used here are $N=100$, $L=110$, and $T=1.6$.

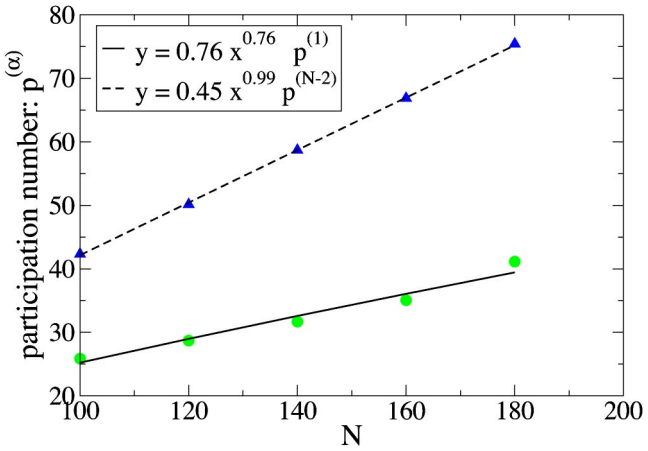

FIG. 19. Time-averaged participation number $p^{(1)}$ and $p^{(N-2)}$ vs particle number N. The parameter settings used here are $L/N=1.1$ and $T=1.6$.

wave numbers. For all the cases checked, no wavelike structure can be identified as for the coordinate part. One may wonder why no modelike collective motion is observed in the momentum part. There are two possibilities. One is that the momentum part does contain information similar to the coordinate part but it is too weak to be detected here due to the strong noise. The other is that there is no similarity between the two parts at all and regular long-wave-length modes exist only in the coordinate part. Further work is needed to clarify which one is correct.

F. Localization properties of LVs

To study the localization of LVs, we employ the participation number, which is defined as

$$p \equiv \left[\sum_{i=1}^{N} (\delta x_i^2 + \delta v_i^2)^2 \right]^{-1} \tag{10}$$

for a Lyapunov vector $(\delta x_i^{(\alpha)}, \delta v_i^{(\alpha)})$ [42]. This is a standard quantity used in the study of disorder-induced localization [43], which roughly measures the number of particles that contribute to the Lyapunov vector. For the homogeneous Lyapunov vector LV_N with $w^2 \equiv \delta x_i^2 + \delta v_i^2 = 1/N$, which corresponds to one of the zero-value LEs, p attains its maximal value N. On decreasing the index of LVs, LEs become larger and larger. Accompanying this, the participation number $p^{(\alpha)}$ decreases as shown in Fig. 18, where the variation of the time-averaged value of $p^{(\alpha)}$ versus index α and $\lambda^{(\alpha)}$, respectively, is plotted. The decrease of $p^{(\alpha)}$ implies that LVs become more and more localized with decreasing α.

One should note that $p^{(N-2)}$ for LV_{N-2} corresponding to the smallest positive Lyapunov exponent is significantly different from $p^{(N)}=N$ for LV_N with $\lambda^{(N)}=0$. In Fig. 18, $p^{(N-2)} \approx 40$ while $p^{(N)}=100$. In the study of space-time chaos, a commonly used measure for quantifying spatiotemporal disorder is the fractal dimension D. For spatiotemporal chaotic systems the associated fractal dimensions D are typically extensive quantities, i.e., they grow proportionally to the system volume V. According to this, a bounded intensive quantity, the dimension correlation length, is defined [44] as $\xi_D = \lim_{V\to\infty}(D/V)^{-1/d}$. Based on the intuitive picture that a spatiotemporally chaotic system is composed of many subsystems and that these subsystems are uncorrelated if they are far apart, it is expected that ξ_D is proportional to the two-point correlation length, which measures the spatial disorder of the system. A particular fractal dimension, the Lyapunov dimension $D_{\mathcal{L}}$, can be easily obtained using the Kaplan-Yorke formalism which relates the Lyapunov dimension to Lyapunov exponents of the system [45]. For a Hamiltonian system like the one studied here, Lyapunov exponents are paired, i.e., $\lambda^{(\alpha)}+\lambda^{(2dN-\alpha)}=0$, due to the symplectic structure of the system [30,31]. According to the Kaplan-Yorke formalism, the Lyapunov dimension for a d-dimensional Hamiltonian spatiotemporally chaotic system will be $D_{\mathcal{L}} = 2dN$ independent of the details of the dynamics. Although $D_{\mathcal{L}}$ defined in such a way is proportional to the volume of the system, i.e., reflects the extensiveness of the system, its value is always a constant irrespective of the temperature change. However, the two-point correlation length does change with the temperature and it even becomes divergent as a phase transition is encountered. In this sense, the Lyapunov dimension $D_{\mathcal{L}}$ and the dimension correlation length ξ_D are only trivially defined here and not good quantities to characterize spatiotemporal Hamiltonian chaos. Here we propose a length scale based on the participation number of LVs:

$$\xi_p^{(\alpha)} \equiv \lim_{V\to\infty} (p^{(\alpha)}/V)^{-1/d} \tag{11}$$

where d is the dimension of the physical space and V is the system volume, which is simply L for our $d=1$ case here. In this definition, the quantity $p^{(\alpha)}$ plays a similar role as the fractal dimension D in the definition of the dimension correlation length ξ_D. According to the fact we mentioned above, $\xi_p^{(N-2)}$ for LV_{N-2} corresponding to the smallest positive Lyapunov exponent is a nontrivial value depending on the state of the system.

Now we first show that $\xi_p^{(N-2)}$ is an intensive quantity like the conventionally defined dimension correlation length ξ_D. Here the particle density $\rho \equiv N/L$ is kept fixed and the particle number N is increased from 100 to 200. The fit of the numerical data in Fig. 19 gives $p^{(N-2)} \sim N^{0.99}$. This tells us $p^{(N-2)}$ is proportional to the system size N, i.e., it is an ex-

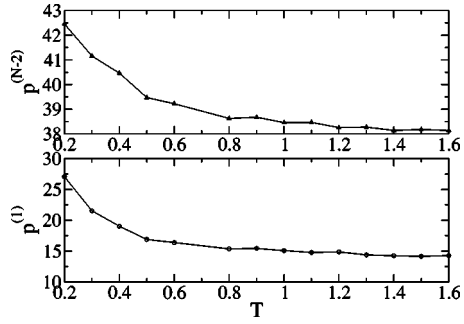

FIG. 20. Time-averaged participation number $p^{(1)}$ and $p^{(N-2)}$ vs temperature T. The parameter setting used here is: $N=200$ and $L=220$.

tensive quantity. Correspondingly, the length scale $\xi_p^{(N-2)}$ is independent of N and is a well-defined intensive quantity. The N dependence of $p^{(1)}$ for the LV corresponding to the largest Lyapunov exponent is shown in the same plot. It is fitted with $p^{(1)} \sim N^{0.76}$, i.e., the Lyapunov vector for the largest LE is highly localized in space [10,32,35]. This is consistent with our above observation (see Fig. 6).

Then we study the temperature dependence of the length scale defined above. For a 200-particle system, the temperature is increased from 0.4 to 1.6. Results of the simulation are shown in Fig. 20, where the variation of $p^{(1)}$ with temperature T is also presented. From the plot, one can see that $p^{(N-2)}$ (and consequently $\xi_p^{(N-2)}$) decreases gradually with the increase in temperature. This agrees with the intuitive expectation that increasing the temperature makes the fluctuation in the system stronger and stronger and renders the system more and more disordered.

IV. CONCLUSION AND DISCUSSION

In this paper, we presented numerical results for the Lyapunov instability of a Lennard-Jones system. Our simulations show that the stepwise structure found in the Lyapunov spectrum of hard-core systems disappears completely here. This is conjectured to be due to the strong fluctuations in the finite-time LEs [10]. A technique [40] based on a spatial Fourier spectral analysis is employed to reveal the hidden long-wavelength structure in LVs. A significantly sharp peak with low wave number is found in the resultant spatial Fourier spectrum for LVs with $\lambda \simeq 0$. This serves as strong evidence that hydrodynamic Lyapunov modes do exist in soft-potential systems [46]. The disappearance of the step structure and the survival of the hydrodynamic Lyapunov modes show that the latter are more robust and essential than the former. Another important finding is that the dispersion relation for hydrodynamic Lyapunov modes, $\lambda^{(\alpha)}$ versus k_{max}, appears to be universal for all the system temperatures and particle densities used in our simulations. This finding will not exclude a possible density dependence of the dispersion relation for systems in the high-density regime [47].

There is a difference between the Lyapunov vectors of our Lennard-Jones system and those for the hard-core system studied before. In hard-core systems, a Lyapunov vector with a near zero Lyapunov exponent can be well fitted by a sinusoidal function $A\sin(kx+\phi)$. Correspondingly the spatial power spectrum of the Lyapunov vector turns out to be nearly a δ function at k. Therefore in this case one can unambiguously classify the Lyapunov vectors by their wave number k. The situation is quite different in the Lennard-Jones system. Here the spatial spectrum of the Lyapunov vector is broadened but still a dominant wave number can be identified. This reminds us of the difference between sound modes in solids and fluids, respectively.

In this study we have simulated a large number of system parameter settings with the density ρ in the range from $1/2$ to $1/40$ and $T=0.2$, 0.3, and 0.4. Here the average distance between nearest neighbors $a \equiv L/N$ is quite large compared to the equilibrium distance r_0 defined through $V'(r_0)=0$. The reason for choosing relatively dilute systems lies in the suspected importance of hyperbolicity for the appearance of the Lyapunov modes [11,48]. In a dilute Lennard-Jones system as considered here, the particles can fly nearly freely for a quite long period of time, then collide with their neighbors, then separate from each other quickly, and so on. These scattering events are similar to what happens in a hard-core system. In contrast, if the particle density is increased to a value comparable to or higher than $\rho_0 \equiv 1/r_0$, the effective interactions among the particles become similar to that of a chain of anharmonic oscillators, where hydrodynamic Lyapunov modes were found to be difficult to observe [48]. This is the reason why dilute systems were selected in our study. The use of relatively low temperatures is due to similar considerations.

In the study of two-dimensional and quasi-one-dimensional hard-core systems, two kinds of hydrodynamic Lyapunov modes are identified [10,15]. One is referred to as transverse and the other is called longitudinal. The former modes do not propagate while the latter can [10]. According to this classification, for the transverse Lyapunov modes, taking the time average can be a useful way to identify the wavelike structure. In contrast to this, the detection of the longitudinal Lyapunov modes, which are the only ones present in one-dimensional systems, is a relatively difficult task since due to its propagation time averaging is no longer a suitable method to suppress the fluctuations [15]. For the case of soft-potential systems, in addition strong fluctuations in local instabilities lead to an occasional mixing among Lyapunov vectors. This is partially reflected in the intermittent time evolution of spatial Fourier spectra of LVs. Therefore the hydrodynamic Lyapunov modes in soft-potential systems are more vague and more difficult to observe [16]. In this work, Fourier spectral analysis has been shown to be quite successful in detecting the hidden wavelike structures in LVs. A more general theoretical consideration of this method is given elsewhere [40].

In studies of the hard-core case, it is conjectured that degeneracies in the Lyapunov spectrum and in wave numbers of hydrodynamic Lyapunov modes are determined by the intrinsic symmetries of the Hamiltonian and the boundary conditions. There is no contradiction between this statement and the results reported here. The crucial point is the lifetime of hydrodynamic Lyapunov modes. The above statement is for the ideal case of pure modes with infinite long lifetime. For the Lennard-Jones system studied here, the strong fluc-

tuation in local instability of trajectories (which is reflected on the wild fluctuations of finite-time Lyapunov exponents) leads to the mutual interaction and mixing among modes, which renders the lifetime of modes becoming finite. On the other hand, Lyapunov exponents are global quantities of the system, which are the result of a time average along a long trajectory wandering all over the phase space allowed. Due to the mixing among modes, the Lyapunov exponents no longer correspond to certain pure modes but to a mixture of several modes. Therefore the degeneration predicted on the basis of a symmetry analysis cannot be seen here. Actually, fluctuations in the local instability of trajectories (fluctuations in the finite-time Lyapunov exponents) do exist in all dynamical systems. For the hard-core systems, however, it is relatively weak in the directions corresponding to $\lambda \approx 0$ (see Fig. 12 in [10] for the comparison of fluctuations in finite-time Lyapunov exponents for the hard-core case and the WCA case). Therefore the mixing among modes is quite rare and weak. In consequence the lifetimes of the modes with $\lambda \approx 0$ are quite long and even longer than the simulation time. Evidence for our arguments above comes from the fact that for hard-core systems the fluctuations in finite-time Lyapunov exponents become stronger for increasing LE (see Fig. 12 in Ref. [10]) and correspondingly the step structure is less pronounced (more inclined) for larger LEs (see Fig. 8 in Ref. [10]).

Until now, only the coordinate part of the LVs was used in the study of hydrodynamic Lyapunov modes. For the case of hard-core system, this is reasonable due to the interesting feature of those LVs corresponding to near-zero LEs found in [12] that the angles between the coordinate part and the momentum part are always small, i.e., the two vectors are nearly parallel. For our soft-potential system, we find that the angles between the coordinate part and the momentum part are no longer as small as in hard-core systems. Even for hard-core systems, recent results show that the two vectors are not always parallel [32]. Therefore it is necessary to reconsider the momentum part of LVs.

We studied also the influence of density and temperature changes on the features of LVs and LEs. One effect of decreasing the density is that the Lyapunov spectrum becomes more and more bent. The relation of the bending in the Lyapunov spectrum to the separation of time scales was discussed recently in the work of Taniguchi and Morriss [32]. It is obvious that the collisions between particles become more and more rare as the density is decreased. They become highly localized events since they happen at only a few places at one moment. Therefore, the time scale of local collision events, which is related to the largest LEs [2], is well separated from that for the collective motion of the system, corresponding to the near-zero LEs. A further point is the sudden jump found in k_{max} of the time-averaged spatial Fourier spectrum of LVs. It divides the whole set of LVs into two groups. The place of this sudden jump is in the regime where the Lyapunov spectrum is strongly bent. Further work is needed to reveal the underlying connection between these phenomena.

ACKNOWLEDGMENTS

We thank H. A. Posch, W. Kob, A. S. Pikovsky, W. Just and A. Latz for fruitful discussions and W. Kob in addition for providing us with his molecular dynamics simulation code, on which our program is built. Financial support from DFG-SFB393 within the project "Long time behavior of large dynamical systems" is gratefully acknowledged.

APPENDIX: ENERGY FLUCTUATION, ZERO-VALUE LYAPUNOV EXPONENTS, AND LYAPUNOV MODES

In this appendix we address in detail the issue of the quality of the zero-value Lyapunov exponents obtained in the numerical simulations and their influence on the Lyapunov modes.

1. Zero-value Lyapunov exponents with large fluctuations

For the one-dimensional Lennard-Jones system studied here, four zero-value Lyapunov exponents are expected [10,12,14]. Two of them correspond to momentum conservation and translational invariance in space. The other two correspond to energy conservation and translational invariance in time. Numerical simulations show that the two corresponding to space translational invariance and momentum conservation are very close to zero since these properties are preserved exactly during the numerical integration of the system dynamics. The Lyapunov exponent $\lambda^{(100)}$ shown in Fig. 3 (and $\lambda^{(101)}$ not shown for symmetry reasons) belongs to this pair. The other pair of Lyapunov exponents ($\lambda^{(99)}$ and $\lambda^{(102)}$) corresponding to the energy conservation and the translational invariance in time deviate from zero to a larger extent. This is due to numerical errors in the simulation of the system and its tangent space dynamics. As we discussed already in Sec. III A, the numerical integration of time-continuous systems on a computer will inevitably introduce deviations from the exact behavior. The resulting fluctuations in the total energy or errors in the tangent space dynamics lead to the observed deviation of this pair of Lyapunov exponents from zero. Obviously the integration step size used to generate the data in Fig. 3 is not small enough to discriminate the LEs which have to be zero ($\lambda^{(99)}$ and $\lambda^{(102)}$) and the nonzero LEs such as the neighboring $\lambda^{(97)}$ and $\lambda^{(98)}$. In principle, one can bring the values of LEs $\lambda^{(99)}$ and $\lambda^{(102)}$ closer to zero by reducing the integration step size and by averaging along a sufficiently long trajectory. Because of the limited computer capacity, we perform numerical simulations for a system with a small number of particles ($N=5$) to support these statements.

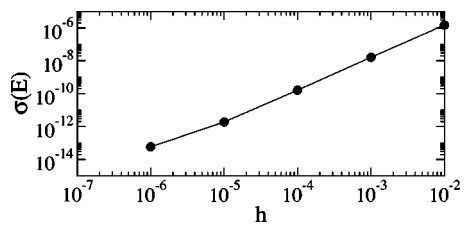

FIG. 21. The standard deviation of the total energy $\sigma(E) \equiv \sqrt{\langle (E-\langle E\rangle)^2\rangle}$ versus the integration step size h, where $\langle \cdots \rangle$ denotes the time average. The parameter settings used here are $N=5$, $L=20$, and $T=0.1$.

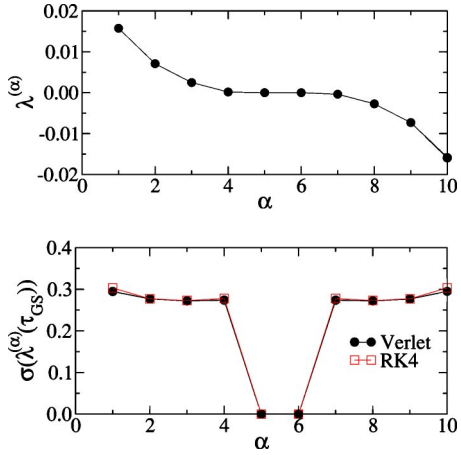

FIG. 22. Lyapunov exponent $\lambda^{(\alpha)}$ (top panel) and the standard deviation of the finite-time Lyapunov exponents $\sigma(\lambda^{(\alpha)}(\tau_{GS})) \equiv \sqrt{\langle[\lambda(\tau_{GS})-\langle\lambda(\tau_{GS})\rangle]^2\rangle}$ (bottom panel) versus the index of the Lyapunov exponents α. The data of $\sigma(\lambda^{(\alpha)}(\tau_{GS}))$ from simulations using the fourth Runge-Kutta integrator are also presented for comparison. τ_{GS} is the period between reorthogonalizations of the offset vectors and here $\tau_{GS}=400h$. The integration step used is $h=0.002$. The length of the trajectory used for time averaging is $\tau_0=1.28\times10^{10}h$.

As can be seen in Fig. 21, the fluctuations in the total energy decrease gradually with decreasing integration step h. For such a system, the Lyapunov exponents $\lambda^{(4)}$ and $\lambda^{(7)}$ correspond to the energy conservation and the time translational invariance. An example of the Lyapunov spectrum of this system is shown in Fig. 22. In Fig. 23, we plot the variation of $\lambda^{(4)}$ with the integration step h. For comparison, the value of $\lambda^{(3)}$ is plotted in the same figure. The numerical value of $\lambda^{(3)}$ is nearly constant irrespective of the change in the integration step h, while the value of $\lambda^{(4)}$ decreases gradually with decreasing h. This figure shows that by varying the step size h the zero-value LEs can be identified.

In the lower panel of Fig. 22 the quantity $\sigma(\lambda^{(\alpha)}(\tau_{GS}))$ measuring the fluctuations of the finite-time Lyapunov exponents is shown. It is nearly zero (of the order 10^{-12}) for Lyapunov exponents $\lambda^{(5)}$ and $\lambda^{(6)}$ which correspond to momentum conservation and space translational invariance. In contrast, $\sigma(\lambda^{(\alpha)})$ for the other pair of zero-value Lyapunov exponents $\lambda^{(4)}$ and $\lambda^{(7)}$ are of the order 0.1, which is of the same order as for their nonzero neighbors $\lambda^{(3)}$ and $\lambda^{(8)}$. Furthermore, the value of the fluctuation strength $\sigma(\lambda^{(\alpha)}(\tau_{GS}))$ is nearly independent of the integration step h (see Fig. 24). Extensive numerical simulations show that these large fluctuations in the short-time behavior of the expansion rates corresponding to the pair of zero-value Lyapunov exponents associated with the energy conservation is not an artificial effect but an inherent quality of the soft-potential system studied. The use of the smoother interaction potentials from Eqs. (3) and (4) or the use of different integration routines leads to basically the same results. The Lyapunov spectrum and the fluctuation $\sigma(\lambda^{(\alpha)})$ as a function of α for a system with $N=40$, $L=160$, and $T=0.8$ are shown in Fig. 25. Here the interaction potential $V(r)$ is of the form as stated in Eq. (4) and the system is integrated with the fourth-order Runge-Kutta algorithm. This figure explicitly shows that the validity of these results is not restricted to small system sizes and that they are independent of the integration algorithms. Our numerical results for the dynamic XY model [16] using the Runge-Kutta algorithm show similar large fluctuations for the short-time Lyapunov exponents corresponding to the energy conservation [49]. These large fluctuations imply the necessity of using long enough trajectories for an accurate determination of the (average) Lyapunov exponents corresponding to energy conservation.

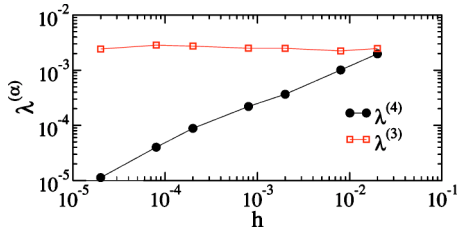

FIG. 23. The values of the exponents $\lambda^{(3)}$ and $\lambda^{(4)}$ versus the integration step size h. Here the reorthogonalization period is fixed at $\tau_{GS}=0.8$ and sufficient long trajectories are used for averaging in order to achieve a good convergence of the data gotten. Other parameters used here are the same as in Fig. 21.

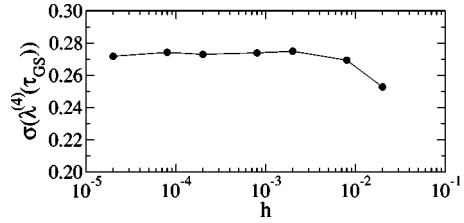

FIG. 24. Fluctuation strength $\sigma(\lambda^{(\alpha)}(\tau_{GS}))$ of the short-time Lyapunov exponent $\lambda^{(4)}(\tau_{GS})$ versus the integration step size h. Other parameters used here are the same as in Fig. 22.

These studies show that two factors are crucial for the quality of the numerical estimation of these zero-value Lyapunov exponents: (1) a small integration step and (2) a long enough trajectory for the average of the finite-time Lyapunov exponents. The former determines the systematic error of the estimation, i.e., the deviation of its mean from zero, while the latter determines the statistical error, i.e., the standard deviation of an ensemble of estimations obtained

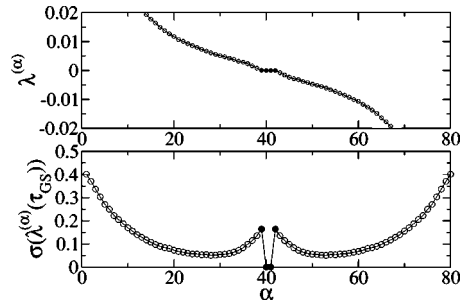

FIG. 25. $\lambda^{(\alpha)}$ and $\sigma(\lambda^{(\alpha)}(\tau_{GS}))$ for a system with $N=40$, $L=160$, and $T=0.8$. The interaction potential is of the form stated in Eq. (4). The system is integrated with the fourth-order Runge-Kutta algorithm.

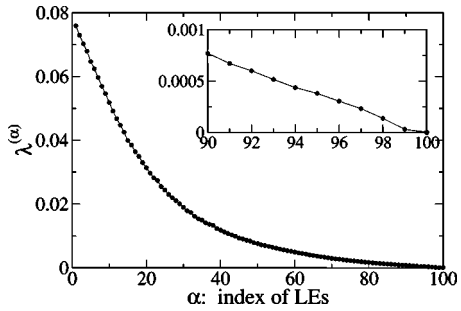

FIG. 26. Lyapunov spectrum for a system with the Stoddard-Ford Lennard-Jones potential in Eq. (3). Apart from the choice of the potential cutoff all the parameters are the same as in Fig. 3.

under the same conditions. Now we discuss what is meant by the phrase "long enough trajectory." Let us denote the estimated value of a Lyapunov exponent from a trajectory of length τ integrated with the step size h as $\lambda(\tau,h)$. A necessary condition for a good estimation is $\sigma(\lambda(h,\tau)) \leqslant \Lambda_0(h)$ where $\sigma(\lambda(h,\tau))$ is the standard deviation of $\lambda(h,\tau)$ and $\Lambda_0(h) \equiv \lim_{\tau\to+\infty}\lambda(h,\tau)$ is the asymptotic value of this zero-value Lyapunov exponent for the integration step size h. The quantity $\sigma(\lambda(h,\tau))$ is related to $\sigma(\lambda(h,\tau_{GS}))$ and can be approximated as $\sigma(\lambda(h,\tau)) \sim (\tau/\tau_{GS})^{-\gamma}\sigma(\lambda(h,\tau_{GS}))$ where γ is a positive constant typically of the order $\frac{1}{2}$. The independence of $\sigma(\lambda(h,\tau_{GS}))$ for small h as shown in Fig. 24 implies that $\sigma(\lambda(h,\tau))$ scales as $(\tau/\tau_{GS})^{-\gamma}$. The decreasing of $\lambda^{(4)}$ with decreasing h as shown in Fig. 23 suggests that $\Lambda_0(h) \sim h^{\eta}$ where η is a positive constant. This amounts to an estimation of the minimal length τ_0 of the trajectory needed for a given integration step size h as $\tau_0 = \text{const} \times h^{-\eta/\gamma}$. This implies that an improvement of the estimation of the zero-value Lyapunov exponent with decreasing step size h as shown in Fig. 24 is possible under the condition that the averaging period is extended (not smaller than $h^{-\eta/\gamma}$) at the same time. Both a smaller integration step and a longer trajectory are necessary conditions for improvement in the estimation of these zero-value Lyapunov exponents. Both measures lead to a fast increase of computational costs. These considerations explicitly provide a means of improving the accuracy of the Lyapunov exponent $\lambda^{(99)}$ in Fig. 3.

Influence of the quality of the zero-value Lyapunov exponent on the Lyapunov modes

While the quality of the zero-value Lyapunov exponents corresponding to energy conservation is quite sensitive to the

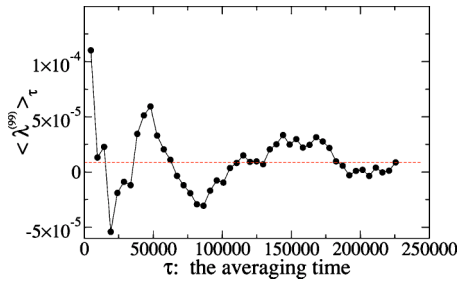

FIG. 27. The part-time-averaged value of $\lambda^{(99)}$ versus the averaging time.

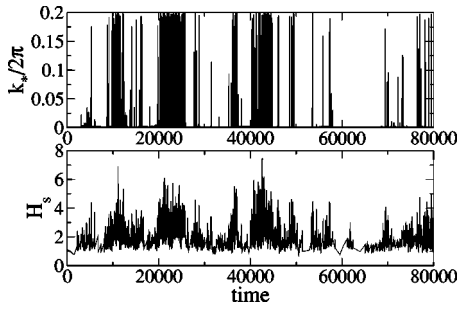

FIG. 28. The time evolution of the peak wave number k_* (upper panel) and the instantaneous spectral entropy $H_s(t)$ (lower panel) for the Lyapunov vector no. 95 of the system used in Fig. 26. The similarity to Fig. 8 is obvious.

details of the numerical integration (step size, trajectory length), the characteristic features of the hydrodynamic Lyapunov modes are quite robust. This fact is exemplified by changing the potential to the Stoddard-Ford form of Eq. (3). Comparing Fig. 3 with Fig. 26 demonstrates the change in the value of $\lambda^{(99)}$, in this case to an improved estimate. On the other hand the corresponding Lyapunov vector turns out to be qualitatively the same as before. The simulations for a system with the interaction potential of Eq. (4) give similar results as we present below.

We emphasize first that the Lyapunov spectrum of a system with Stoddard-Ford Lennard-Jones potential [Eq. (3)], as shown in Fig. 26, also does not exhibit the step structures observed in hard-core systems. Secondly, we depict in Fig.

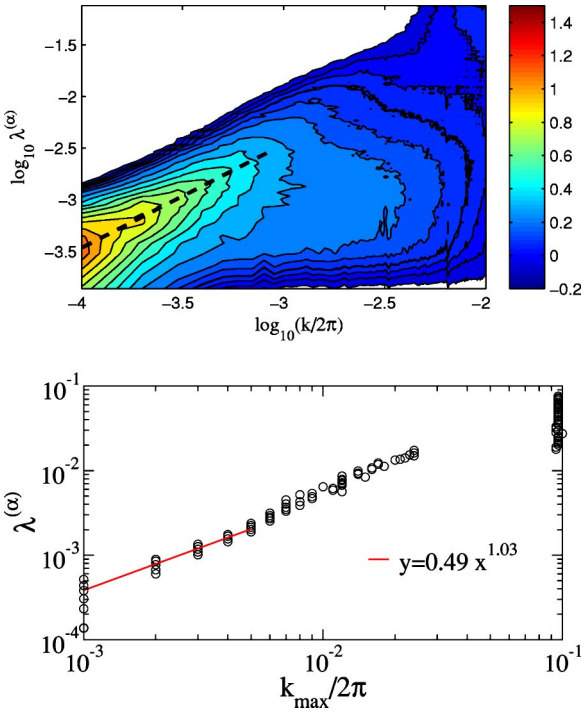

FIG. 29. (Color online) The contour plot of the spectrum $S_{uu}^{(\alpha)}$ (upper panel) and the dispersion relation $\lambda^{(\alpha)}$ versus k_{max} (lower panel) for the system shown in Fig. 26. See Figs. 11 and 12 for similar results of the model with the interaction potential stated in Eq. (2).

27 the convergence of $\lambda^{(99)}$ with increasing averaging time. It shows that the numerically estimated value of this Lyapunov exponent behaves irregularly as a function of the averaging time and decreases only in the mean. This confirms the need for increasing the averaging time to obtain an accurate estimate of the Lyapunov exponent $\lambda^{(99)}$ but that one can get very good estimates also accidentally.

The peak value k_* and the spectral entropy $H_s(t)$ of the instantaneous spectrum $s_{uu}^{(\alpha)}(k)$ for Lyapunov vector no. 95 of the above system are plotted against time in Fig. 28. The intermittent behavior of both quantities is similar to the one shown in Fig. 8.

The contour plot of the spectrum $S_{uu}^{(\alpha)}$ is shown in Fig. 29. The ridge structure in the small-k and -λ regime indicates the existence of the hydrodynamic Lyapunov modes. The λ-k dispersion relation extracted is quite close to a linear one. The similarity to Figs. 11 and 12 is obvious.

Our results above show that the Lyapunov spectrum, especially the pair of zero-value Lyapunov exponents corresponding to energy conservation, is sensitive to the details of the models considered, while the behavior of the Lyapunov vectors is quite robust. At least, the existence of hydrodynamic Lyapunov modes is universal irrespective of these changes.

[1] J.-P. Eckmann and D. Ruelle, Rev. Mod. Phys. **57**, 617 (1985); E. Ott, *Chaos in Dynamical Systems* (Cambridge University Press, Cambridge, U.K., 1993).

[2] N. S. Krylov, *Works on the Foundations of Statistical Mechanics* (Princeton University Press, Princeton, NJ, 1979).

[3] P. Gaspard, *Chaos, Scattering, and Statistical Mechanics* (Cambridge University Press, Cambridge, U.K., 1998).

[4] J. P. Dorfman, *An Introduction to Chaos in Nonequilibrium Statistical Mechanics* (Cambridge University Press, Cambridge, U.K., 1999).

[5] D. J. Evans and G. P. Morriss, *Statistical Mechanics of Nonequilibrium Liquids* (Academic, New York, 1990).

[6] Wm. G. Hoover, *Computational Statistical Mechanics* (Elsevier, New York, 1991).

[7] Wm. G. Hoover, *Time Reversibility, Computer Simulation, and Chaos* (World Scientific, Singapore, 1999).

[8] Lj. Milanović, H. A. Posch and Wm. G. Hoover, Mol. Phys. **95**, 281 (1998), H. A. Posch and R. Hirschl, in *Hard Ball Systems and the Lorentz Gas*, edited by D. Szasz, EMS Vol. 101 (Springer, Berlin, 2000), p. 269.

[9] H. A. Posch and Ch. Forster, in *Collective Dynamics of Nonlinear and Disordered Systems*, edited by G. Radons, W. Just, and P. Häussler, (Springer Berlin, 2004), p. 309.

[10] C. Forster, R. Hirschl, H. A. Posch, and Wm. G. Hoover, Physica D **187**, 294 (2004).

[11] J.-P. Eckmann and O. Gat, J. Stat. Phys. **98**, 775 (2000).

[12] S. McNamara and M. Mareschal, Phys. Rev. E **64**, 051103 (2001); M. Mareschal and S. McNamara, Physica D **187**, 311 (2004).

[13] A. de Wijn and H. van Beijeren, e-print nlin.CD/0312051.

[14] T. Taniguchi and G. P. Morriss, Phys. Rev. E **65**, 056202 (2002).

[15] T. Taniguchi and G. P. Morriss, Phys. Rev. E **68**, 026218 (2003).

[16] Wm. G. Hoover, H. A. Posch, C. Forster, C. Dellago, and M. Zhou, J. Stat. Phys. **109**, 765 (2002).

[17] M. C. Cross and P. C. Hohenberg, Rev. Mod. Phys. **65**, 851 (1993).

[18] S. D. Stoddard and J. Ford, Phys. Rev. A **8**, 1504 (1973).

[19] W. Kob and H. C. Andersen, Phys. Rev. E **51**, 4626 (1995).

[20] G. Benettin, L. Galgani, and J. M. Strelcyn, Phys. Rev. A **14**, 2338 (1976).

[21] I. Shimada and T. Nagashima, Prog. Theor. Phys. **61**, 1605 (1979).

[22] H. A. Posch and W. G. Hoover, Phys. Rev. A **38**, 473 (1988).

[23] A. Pikovsky, Chaos **3**, 225 (1993).

[24] C. Dellago, W. G. Hoover, and H. A. Posch, Phys. Rev. E **65**, 056216 (2002).

[25] J. P. Boon and S. Yip, *Molecular Hydrodynamics* (McGraw-Hill, New York, 1980).

[26] M. P. Allen and D. J. Tildesley, *Computer Simulations of Liquids* (Oxford Science, Oxford, 1987).

[27] F. H. Stillinger, Phys. Rev. E **52**, 4685 (1995).

[28] V. I. Oseledec, Trans. Mosc. Math. Soc. **19**, 197 (1968).

[29] S. V. Ershov and A. B. Potapov, Physica D **118**, 167 (1998).

[30] D. J. Evans, E. G. D. Cohen, and G. P. Morriss, Phys. Rev. A **42**, 5990 (1990).

[31] C. P. Dettmann and G. P. Morriss, Phys. Rev. E **53**, R5545 (1996).

[32] T. Taniguchi and G. P. Morriss, Phys. Rev. E **68**, 046203 (2003).

[33] Y. Pomeau, A. Pumir, and P. Pelce, J. Stat. Phys. **37**, 39 (1984); K. Kaneko, Physica D **23**, 436 (1986).

[34] G. Giacomelli and A. Politi, Europhys. Lett. **15**, 387 (1991).

[35] A. Pikovsky and A. Politi, Nonlinearity **11**, 1049 (1998); Phys. Rev. E **63**, 036207 (2001).

[36] W. Pesch, D. A. Egolf, I. V. Melnikov, and R. E. Ecke, Nature (London) **404**, 733 (2000).

[37] Lj. Milanović, H. A. Posch, and Wm. G. Hoover, Chaos **8**, 455 (1998).

[38] W. H. Hess, S. A. Teukolsky, W. T. Vetterling, and B. P. Flannery, *Numerical Recipes in Fortran 77* (Cambridge University Press, Cambridge, U.K., 1992), p. 569.

[39] R. Livi, M. Pettini, S. Ruffo, M. Sparpaglione, and A. Vulpiani, Phys. Rev. A **31**, 1039 (1985).

[40] G. Radons and H. L. Yang, e-print nlin.CD/0404028.

[41] J.-P. Eckmann, C. Forster, H. A. Posch, and E. Zabey, e-print nlin.CD/0404007.

[42] Here we follow Ref. [35] to construct a scalar variable $\delta x_i^2 + \delta v_i^2$ to study the localization of LVs.

[43] D. J. Thouless, Phys. Rep. **13**, 93 (1974); F. Wegner, Z. Phys. B **36**, 209 (1979).

[44] M. C. Cross and P. C. Hohenberg, Rev. Mod. Phys. **65**, 851 (1993); C. S. O'Hern, D. A. Egolf, and H. S. Greenside Phys. Rev. E **53**, 3374 (1996).

[45] J. Kaplan and J. A. Yorke, Lecture Notes in Mathematics Vol.

730 (Springer, Berlin, 1979), p. 204.
[46] Hydrodynamic Lyapunov modes were recently also found in other soft-potential fluids, namely, in fluids with the Weeks-Chandler-Anderson (WCA) interaction potential; Ch. Forster and H. A. Posch, nlin.CD/0409019.
[47] The density dependence of the dispersion relation for hard-core systems was studied in [41]. In the high-density regime the slopes of the dispersion relation change with the density.
[48] See the citation of Politi's work on this point in [11].
[49] H. L. Yang and G. Radons (unpublished).